# ELECTRIC VEHICLE PROPULSION SYSTEM

*** Karim N. Mobariz, ** Ahmed M. Youssef,**
***** Mohamed Abdel-Rahman**
** Ph.D. Candidate,*
*Ain Shams University, Cairo, Egypt*
** Associate Professor,
*Egyptian Armed Forces, Cairo, Egypt*
*** Associate Professor, Electrical Power Engineering,
*Ain Shams University, Cairo, Egypt*



## ABSTRACT

*Global pollution and radiations due to greenhouse gases are of serious concern in densely populated urban areas. Electric vehicles are considered one of the pillars of eco-friendly solutions since they produce no exhaust gases. Therefore this paper carries out the study and the improvement in overall performance of an electric vehicle propulsion system, which consists of electric energy supply and traction systems. The supply system constitutes the fuel-cell stack and the DC-DC buck converter, while the traction system constitutes the Brushless Direct Current (BLDC) motor, its voltage source inverter and drive system.*

***Keywords:*** *buck converter; fuel cell; BLDC; fuzzy logic controller; speed control; current control*

## INTRODUCTION

Fossil-fuel pollutants being pumped into the atmosphere and greenhouse gas emissions are estimated to be responsible for around 1.3 million deaths every year. The environmental impact of combustion of gasoline and other fossil fuels has renewed the researchers to focus on electric vehicles. Mass adoption of electric vehicles would lead to substantial reductions in greenhouse gas emissions, according to a study from Newcastle University and reports from the Electric Power Research Institute (EPRI) and the Natural Resources Defense Council (NRDC) [1, 2].

Electric vehicle propulsion system consists of electric energy supply and traction systems. Although batteries are probably the most widely used energy storage devices [3], they are not universal solutions for powering electric vehicles due to inherent limitations in recharging time and lifetime. Considering the role of hydrogen in our future society, clean fuel cell technology is an attractive alternative since fuel cells emit essentially no pollutants and have high-power density and quick start. Unfortunately, fuel cells are sensitive to sudden changes in the loads; i.e. when the load increases, the fuel cell stacks voltage will drop steeply, which will affect the output voltage. Therefore, a DC-DC buck converter is proposed to maintain the fuel cell stacks output voltage to a desired value. An optimized proportional-integral-derivative (PID) controller is suggested for the

DC-DC buck converter to ensure a constant output voltage and to reject the disturbance from load and fuel cells stacks. Hence, a fuel cell stack, a DC-DC buck converter and its associated controller will constitute the electric energy supply system.

Electric motors play significant role in electric vehicles. Mainly, there are two types of DC motors used in industry. The first one is the conventional DC motor where the flux is produced by the current through the field coil of the stationary pole structure. The second type is the BLDC motor where the permanent magnet provides the necessary air gap flux instead of the wire-wound field poles [4]. Unlike conventional DC motor which uses mechanical commutator and brushes, BLDC motor uses electronic commutation system which consists of an inverter and a position sensor that detects rotor position for proper commutation of current. According to this structure, brush maintenance free operation is achieved, and problems resulting from mechanical wear of brushes and commutators are improved by changing the position of rotor and stator in DC motor. Therefore BLDC motors have gained many advantages over conventional DC motors such as higher reliability and efficiency, compactness, longer operating life, higher dynamic response, better speed versus torque characteristics, noiseless operation, and higher torque-to-weight ratio. Due to these advantages, BLDC motors are preferred for the electric vehicle application as traction motors, and hence the electric vehicle traction system is constituted of the BLDC traction motor together with voltage source inverter.

High performance electric motor drive systems are central to modern electric vehicle propulsion systems [5]. The benefits accruing from the application of such drives are precision control of torque, speed and position which promote superior electric vehicle dynamical performance [6]. Designing and controlling of a BLDC motor drive system requires an accurate model of the motor, therefore modeling of a BLDC motor with a trapezoidal back-Electro Magnetic Force (back-EMF) waveform shape along with a control system for its speed and current is presented. A fuzzy logic controller is used for designing the speed control system due to its robustness to plant parameter changes and to its better noise rejection capabilities, while an optimized PI controller is used for designing the current control system.

The paper is organized in six sections: Section 2 describes briefly the components of the electric vehicle propulsion system. Section 3explains the principle of operation of the traction system components. Designing the controllers of the BLDC motor drive is detailed and simulation results are explained in Section 4.Section 5 details the operational characteristics and the mathematical modeling of the supply system components, followed by the design of the buck converter controller and its simulation results. Finally, the paper concludes with a brief summary in Section 6.

## ELECTRIC VEHICLE PROPULSION SYSTEM DESCRIPTION

Fig. 1 shows the proposed electric vehicle propulsion system. It consists of electric energy supply and traction systems. The supply system constitutes the fuel-cell stack and the DC-DC buck

converter, while the traction system constitutes the BLDC motor, its voltage source inverter and drive system.

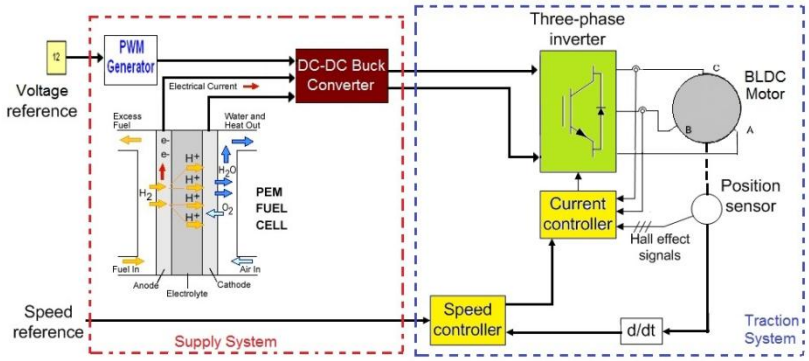


Figure 1 Electric vehicle propulsion system

## TRACTION SYSTEM COMPONENTS

Complete electric vehicle traction system usually consists of BLDC motor, inverter bridge, rotor position sensor, controller and driver circuit. A BLDC motor is synchronous motor with permanent magnets on the rotor and armature windings on the stator. It is powered by a DC electric source via an integrated inverter/switching power supply, which produces an AC electric signal to drive the motor, i.e. the motor accomplishes commutation electronically. The commutation instants are determined by the rotor position. Detecting the rotor position in BLDC motors is performed either by position sensors like Hall sensor, position encoder and resolver etc. or by sensorless techniques. A three-phase BLDC motor has three stator windings, which are oriented 120$^{o}$ apart. When the motor rotates, each winding generates a voltage called back-EMF, which has an opposite polarity to the energized voltage. There are two types of stator windings: trapezoidal and sinusoidal, which refers to the shape of the back-EMF signal. Trapezoidal motor is a more attractive alternative for most applications due to its simplicity, lower price and higher efficiency [7]. The Simulink diagram; Fig. 2, is drawn based on the standard electrical and mechanical equations of the BLDC motor found in a variety of standard references (see for example [8, 9]).

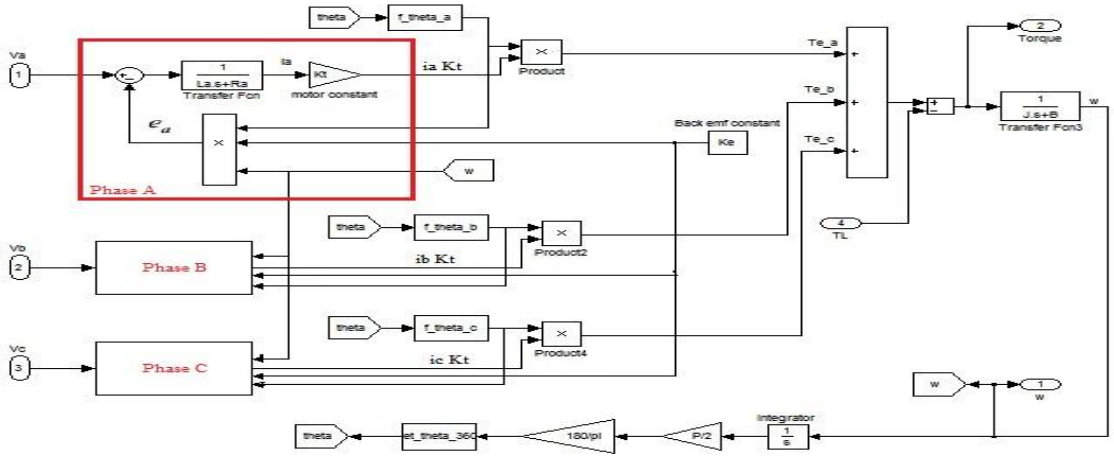


Figure 2 Simulink model of BLDC motor

A three-phase trapezoidal stator windings BLDC motor requires three Hall sensors to detect its rotor position, each hall sensor is typically mounted 120$^o$ apart and produces "1" whenever it faces the North pole of the rotor, i.e. every 60$^o$ rotation. Therefore, it takes six steps to complete an electrical cycle. The Hall sensor signals are fed to the control circuit which controls the direction and speed of the motor by producing PWM signals for triggering the electronic switches; MOSFET or IGBT, of the six-step inverter bridge via an interface driver. The inverter bridge structure is shown in Fig. 3. In six-step inverter operation, only two winding are energized at a time. Each step rotates at 60$^o$, which six paths make a full 360$^o$ rotation. One full 360$^o$ loop is able to control the current, due to the fact that there is only one current path. The switching sequence, the current direction and the position signals are shown in Table I.

Table I Switching sequence of BLDC motor

| Switching interval | Sequence no. | Position sensors | | | Switch closed | | Phase current | | |
|---|---|---|---|---|---|---|---|---|---|
| | | Hall a | Hall b | Hall c | | | a | b | C |
| 330-30 | I | 1 | 0 | 1 | S5 | S4 | off | - | + |
| 30-90 | II | 1 | 0 | 0 | S1 | S4 | + | - | off |
| 90-150 | III | 1 | 1 | 0 | S1 | S6 | + | off | - |
| 150-210 | IV | 0 | 1 | 0 | S3 | S6 | off | + | - |
| 210-270 | V | 0 | 1 | 1 | S3 | S2 | - | + | off |
| 270-330 | VI | 0 | 0 | 1 | S5 | S2 | - | off | + |

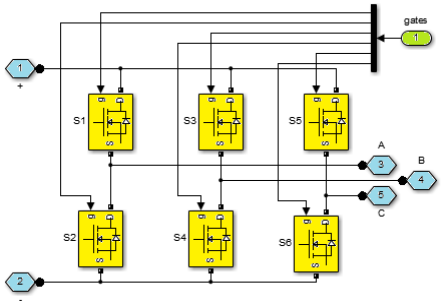


Figure 3. Inverter bridge structure

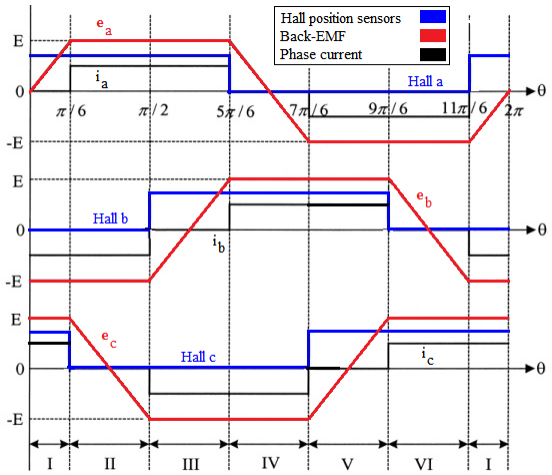


Figure 4. back-EMF, Hall position sensors and phase current

The back-EMF "e" is a function of rotor position "θ" and has the amplitude $\mathbf{E = K_e \cdot \omega}$ where $\mathbf{K_e}$ is the back-EMF constant and $\boldsymbol{\omega}$ is the rotor mechanical speed.

Fig.4 shows an example of Hall sensor signals with respect to back-EMF and the phase current. The parameters used for the modeling BLDC motor (part no.: 80190502) are shown in Table II [10].

Table II BLDC motor technical specifications

| | | | |
|---|---|---|---|
| Max. speed | 8000 rpm | Number of poles | 4 |
| Torque peak in | 1160 mN.m | Terminal resistance | 0.24Ω |
| Max. continuous torque | 463 mN.m | Torque constant | 50.4 mN.m/A |
| Motor constant | 103 mN.m/$W^{1/2}$ | Back-EMF constant | 0.0504 V/(rad/s) |
| Rotor inertia | 230 g.$cm^2$ | Inductance | 0.6mH |

## Motor Drive System Controllers

In most traction applications, BLDC motor drive system controllers include both a speed controller and a current controller to control the motor performances. Simulink model of the traction system is shown in Fig. 5, where a cascaded speed control scheme consisting of an inner current control loop and an outer speed control loop is employed. The inner current control is designed using a PI-type controller with pulse width modulator to smooth the torque response curve with changes in loads, while a Fuzzy Logic Controller (FLC) is designed for the outer speed control loop to adjust the BLDC motor speed.

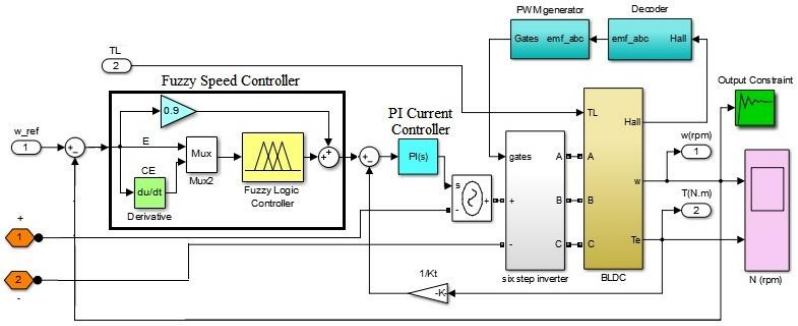


Figure 5. Simulink model of the traction system

### *A. Current Controller*

A mathematical description of the PI controller is:

$$u(t) = K_p\, e(t) + K_i \int_0^t e(\tau)\, d\tau \qquad (1)$$

where Kp and Ki are the proportional and integral gains, respectively. As shown in Fig. 5, the phase currents are converted to equivalent dc-link current value; $I = \frac{T_e}{K_t}$, This value is subtracted from a reference value calculated from the referenced torque signal; produced by the speed controller. This current error e(t) is fed to the PI current controller and its output signal u(t) is compared to sawtooth ramp generated by ramp generator; as will be discussed in details in Section. The output of the comparator is a high or low signal which serves as a chopping for the inverter.

Unlike traditional trial-and-error methods for obtaining PI parameters, a GUI provided by Simulink Response Optimization Software (SROS) is used to tune the parameters within a Simulink model to meet time-domain performance requirements by graphically placing constraints within a time-domain window; as shown in Fig. 5 [11]. SROS automatically converts time-domain constraints into a constrained optimization problem and then solves the problem using any optimization technique. In this paper, gradient descent optimization technique is used.
After a few iterations, the optimal and feasible PI gains obtained were 9 and 0.015 related to Kp and Ki, respectively.

### *B. Speed Controller*

The speed controller is used to compare the desired reference speed ($\omega_{ref}$) value with the actual speed of the motor ($\omega$). The angular velocities used as referenced velocities are shown in Table III.

Table III. Motor angular velocities

| *Process* | *Time interval [min]* | *Rotor speeds (rpm)* |
|---|---|---|
| 1 | 0 – 2 | 1800 |
| 2 | 2 – 10 | 2500 |
| 3 | 10 – 20 | 1800 |
| 3 | 20 – 65 | 3000 |
| 4 | 65 – 110 | 1800 |
| 5 | 110–118 | 2500 |
| 6 | 118–120 | 1800 |
| 7 | 120 | 0 |

A combination between FLC and proportional controller is used to control the speed of the BLDC motor. FLC is designed using Mamdani style fuzzy inference system. FLC is chosen for its robustness to plant parameter changes than classical controllers and for its capability to reject noises. The basic structure of a FLC includes four blocks: (1) fuzzifire which converts input data (real number or crisp variables) to suitable linguistic values, (2) rule base, (3) inference engine which infer a fuzzy control action from knowledge of the rule base and the linguistic variable definition, and (4) defuzzifier which transforms the linguistic variables again to crisp output.

Here FLC has two inputs and one output. These are speed error (E) and change in speed error (CE) and reference current control signal, respectively. As shown in Fig. 5, speed error is the difference between reference speed ($\omega_{ref}$) and the actual speed of the motor ($\omega$). There are seven clusters in the membership functions as shown in Fig. 6. The definitions of the seven linguistic variables as well as the rule base are presented in Table IV.

Table IV. Rule base of fuzzy controller and linguistic variables definitions

| *E* / *CE* | *NB* | *NM* | *NS* | *Z* | *PS* | *PM* | *PB* |
|---|---|---|---|---|---|---|---|
| NB | NVB | NVB | NVB | NB | NM | NS | Z |

| | |
|---|---|
| V | Very |

| | | | | | | | |
|---|---|---|---|---|---|---|---|
| NM | NVB | NVB | NB | NM | NS | Z | PS |
| NS | NVB | NB | NM | NS | Z | PS | PM |
| Z | NB | NM | NS | Z | PS | PM | PB |
| PS | NM | NS | Z | PS | PM | PB | PVB |
| PM | NS | Z | PS | PM | PB | PVB | PVB |
| PB | Z | PS | PM | PB | PVB | PVB | PVB |

| | |
|---|---|
| N | Negative |
| P | Positive |
| S | Small |
| M | Medium |
| B | Big |
| Z | Zero |

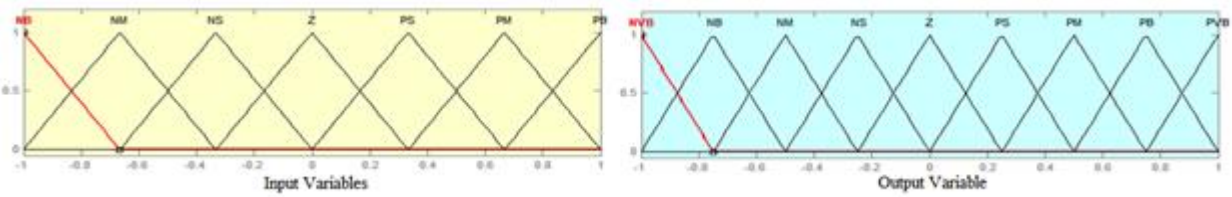


Figure 6. Membership functions of inputs (E, CE) and output of FLC

Fig. 7 illustrates that the actual rotor angular velocities follow the reference ones, while Fig. 8 shows that motor torque fulfils the specifications in Table II.

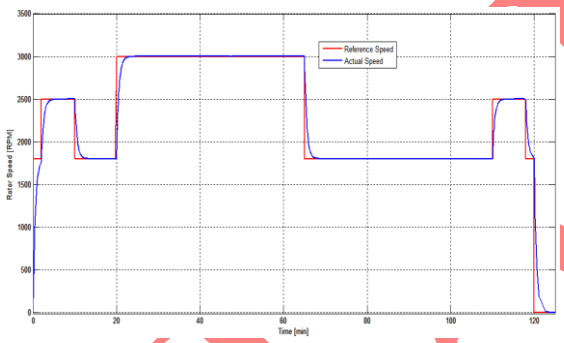


Figure 7. Controlled motor speed

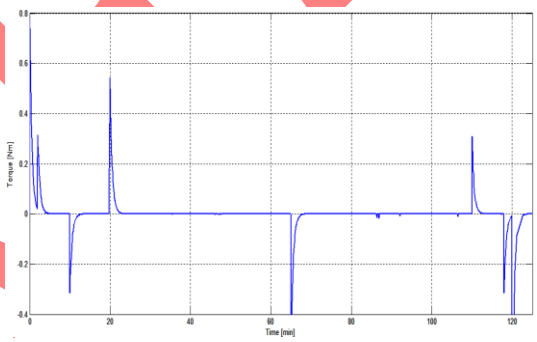

Figure 8. Controlled motor torque

## SUPPLY SYSTEM COMPONENTS MODELLING

### *A. Polymer electrolyte \ proton exchange membrane fuel cell*

A fuel cell is an electro-chemical device that converts chemical energy into electrical energy and heat as a byproduct. The fuel cell will continuously deliver electric power as long as fuel is supplied. The most commonly used fuels are hydrogen and oxygen. There are many types of fuel cells available today: such as proton exchange membrane fuel cells, alkaline fuel cells, phosphoric acid fuel cells, solid oxide fuel cells, and molten carbonate fuel cells [12, 13]. In this paper, Polymer Electrolyte Membrane or Proton Exchange Membrane fuel cells (PEMFCs) are used because of their comparatively high efficiency, high energy density, low working temperature ($30-100^{o}C$), compactness, easy and safe operational modes, in addition of being available in the marketplace for a variety of different systems [14, 15].

A PEMFC consists of a solid polymer electrolyte membrane sandwiched between two electrodes (anode and cathode), as shown in Fig. 9. When the hydrogen is injected at the anode and enters the electrolyte, it ionizes [12, 16].

$$\text{Anode: } H_2 \rightarrow 2H^+ + 2e^- \tag{2}$$

Only protons are allowed to pass through the electrolyte, therefore the protons move across the electrolyte to the cathode to rejoin with oxygen, while the freed electrons from the hydrogen atoms travel through an external circuit to recombine with oxygen at the cathode.

$$\text{Cathode: } O_2 + 4H^+ + 4e^- \rightarrow 2H_2O \tag{3}$$

Therefore, the overall chemical reaction becomes:

$$2H_2 + O_2 \rightarrow 2H_2O + \text{Electricity + heat} \tag{4}$$

i.e., hydrogen gas is recombined with oxygen gas producing electricity with water vapor as emission. A closed loop system could be operated whereby the water from of the PEMFC can be electrolyzed into oxygen and hydrogen for later re-use. Oxygen is generally obtained from the surrounding air.

Typically, a single fuel cell produces voltage between 0 and 1V based on the polarization *I-V* curve; shown in Fig. 10. The relationship between output voltage and load current is given as:

$$V = E - \underbrace{(i + i_n)r}_{\text{Ohmic loss}} - \underbrace{A \ln\left(\frac{i + i_n}{i_0}\right)}_{\text{Activation loss}} + \underbrace{B \ln\left(1 - \frac{i + i_n}{i_l}\right)}_{\text{Concentration loss}} \tag{5}$$

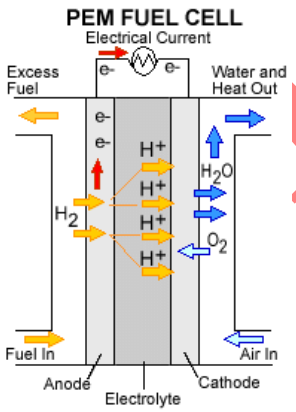


Fig 9. Single PEMFC

Table V. Single PEMFC parameters

| ***Parameter*** | ***Value*** |
|---|---|
| Open circuit voltage $E$ | 1.2 volt |
| Internal current density $i_n$ | 2 mA/ $cm^2$ |
| Internal resistance $r$ | 0.00003 kΩ.$cm^2$ |
| Activation losses constant $A$ | 0.06 volt |
| Exchange current density $i_0$ | 0.067 mA/ $cm^2$ |
| Concentration losses constant $B$ | 0.05 volt |
| Limit current density $i_l$ | 900 mA/ $cm^2$ |

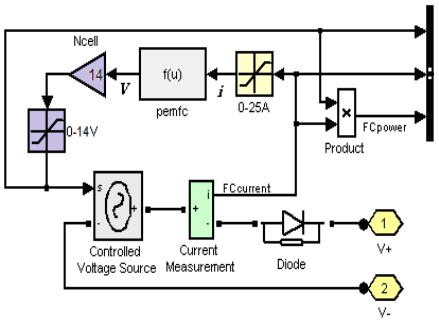


Figure 11. Simulink model of PEMFC stack

It is well known that fuel cell produces an inconstant voltage output when current changes suddenly, therefore a DC-DC buck converter is proposed to maintain the fuel cell stacks output voltage to a desired value.

### *B. Buck converter*

Buck converter is a type of switching-mode power supply which is used for stepping-down DC voltage level. It uses two switches (a MOSFET and a diode), an inductor and a capacitor. In Fig. 12, when a positive signal is applied at the MOSFET gate (g > 0), the DC input voltage $V_{in}$ from the PEMFC is allowed to charge the inductor and to supply output voltage $V_{out}$ across the output capacitor $C_{out}$. Charging will continue till $V_{out}$ reaches to reference voltage $V_{ref}$, then the control part turns OFF the switch (g = 0). The inductor will then change its voltage polarity and the current will flow in the same direction through the diode which is turned ON by switch controller part. Discharging will continue until $V_{out}$ reaches below $V_{ref}$, then control part again turns ON the MOSFET to compensate $V_{out}$ drop and this cycle continues until complete regulation of $V_{out}$ [17]. This process is accomplished by sensing the output voltage of the circuit by means of a negative feedback loop to the pulse-width-modulation (PWM) generator which controls the ON and OFF states of the MOSFET switches.

Controlling the switches, or in other words changing the duty cycle $D$ to keep $V_{out}$ equal to $V_{ref}$ can be explained as follows: the error voltage ($V_E = V_{ref} - V_{out}$) is compared to sawtooth ramp $V_{saw}$ generated by ramp generator, if voltage $V_E$ is higher than $V_{saw}$ as in Fig. 13, the PWM generator reduces the duty cycle by holding ON the MOSFET gate for a short time of every cycle. While $V_E$ is lower than $V_{saw}$, the PWM generator increases the duty cycle by holding ON the gate for the most of cycle to rectify the output voltage.

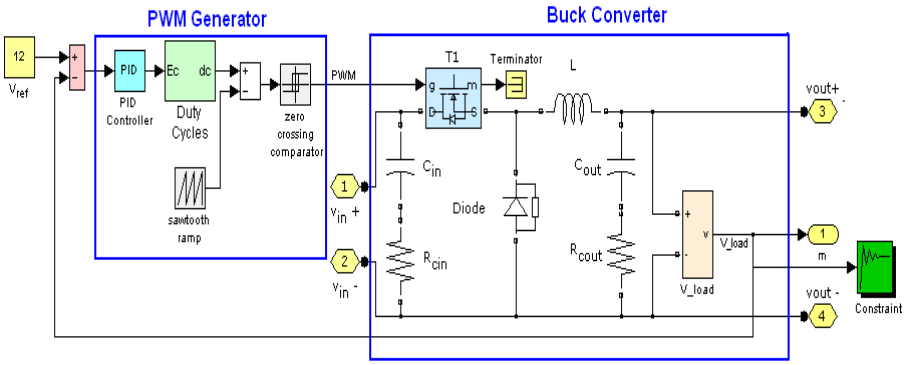


Figure 12. Buck converter control loop

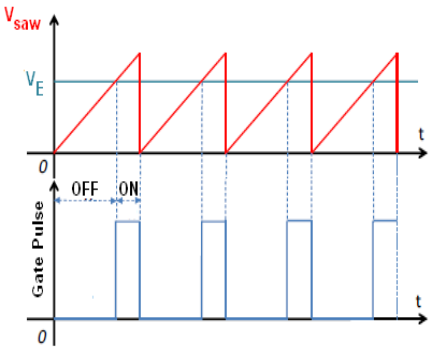


Figure 13. PWM controlled input voltage

The duty cycle is the ratio of the output voltage to the input voltage considering the voltage applied on diode $V_F$ and MOSFET $V_{out}$ as shown in Eq.(6), and its value lies between 0 to 1.

$$D = \frac{V_{out} + V_F}{V_{in} - V_{RDSon}} \tag{6}$$

The selection criterion of the buck converter elements is explained as follows: the output capacitor ($C_{out}$) is chosen to filter the switching ripple; its capacitance must be large enough so that its impedance is much smaller than the load at the switching frequency, allowing most of the ripple current to flow through the capacitor, not the load. The output capacitor's equivalent series resistance $R_{Cout}$ must also be taken into account because its parasitic resistance causes additional voltage ripple [18]. The output voltage ripple $V_{ripple}$ and the minimum output current $I_{min}$ are assumed to be 1% of $V_{out}$ and 10% of $I_{out}$, respectively:

$$C_{out} \geq C_{out\,\min} \qquad C_{out\,\min} = \frac{2 * I_{\min} * T}{8 * V_{ripple}} \tag{7}$$

The input capacitor ($C_{in}$) deals with highest ripple current. An acceptable level of the input voltage ripple $V_{rippleIN}$ is assumed to be 5% of $V_{in}$.

$$C_{in} \geq C_{in\,\min} \qquad C_{in\,\min} = \frac{I_{peak} * T}{8 * V_{rippleIN}} = \frac{I_{peak} * T}{8 * (0.05 * V_{in})} \tag{8}$$

The minimum inductor value ($L_{min}$) is calculated as follows:

$$C_{in} \geq C_{in\,\min} \qquad C_{in\,\min} = \frac{I_{peak} * T}{8 * V_{rippleIN}} = \frac{I_{peak} * T}{8 * (0.05 * V_{in})} \tag{9}$$

According to the above equations, the calculated buck converter parameters are listed in Table VI.

Table VI. Buck converter parameters

| ***Parameter*** | ***Symbol*** | ***Value*** | ***Unit*** | ***Parameter*** | ***Symbol*** | ***Value*** | ***Unit*** |
|---|---|---|---|---|---|---|---|
| Output voltage of converter | $V_{out}$ | 12 | V | Duty cycle | $D$ | 0.914 | |
| Input voltage of converter | $V_{in}$ | 14 | V | Switching period | $T$ | 20 | μ sec |
| Nominal output current | $I_{out}$ | 6 | A | On-time of the switch | $T_{on}$ | 18.284 | μ sec |
| Peak switching current | $I_{peak}$ | 6.6 | A | Inductor value used | $L$ | 5665 | μH |
| Maximum allowable peak-to-peak ripple | $V_{ripple}$ | 0.12 | V | Output bank capacitance | $C_{out}$ | 550 | μF |
| Drain to source resistance at switching on | $R_{DSon}$ | 0.1 | Ω | Internal resistance of ($C_{out}$) used | $R_{Cout}$ | 0.015 | Ω |
| Forward voltage drop across diode | $V_F$ | 0.25 | V | Capacitance of input bank | $C_{in}$ | 500 | μF |
| Voltage drop across $R_{DSon}$ | $V_{RDSon}$ | 0.6 | V | Internal resistance of ($C_{in}$) used | $R_{Cin}$ | 0.1 | Ω |

### *C.* ***Buck converter controller design and simulation results***

Buck converter controller design has centered mainly on simple, linear, PID controller. Although a PID controller is one of the earlier control strategies, it still has a wide range of applications in industrial control due to its easily implementation in the field environment.
A mathematical description of the PID controller is:

$$u(t) = K_p\, e(t) + K_i \int_0^t e(\tau)\, d\tau + K_d \frac{d\, e(t)}{d\, t} \qquad (10)$$

where the input signal $e(t)$ is the error voltage ($V_E = V_{ref} - V_{out}$), $K_p$, $K_i$, and $K_d$ are the proportional, integral, and derivative gains, respectively, while the controller output $u(t)$ is the input signal to the duty cycle block; as shown in Fig. 12. Again as in Section 4, instead of using hand-tuning method, parameters of PID controller are tuned using SROS with gradient descent optimization technique to meet time-domain performance requirements by tracking and closely matching a reference signal.

Due to the sudden variations in motor speeds, the output current of the fuel cell changes suddenly and consequently the fuel cell produces an inconstant voltage output. Fig. 14 shows that the designed optimized PID controller for the proposed DC-DC buck converter is capable to convert the fuel cell output voltage into standard DC; 12V, and to achieve a satisfactory transient

behavior. Moreover, it significantly decreases the ripples of the output current compared to those of the input current as obvious from Fig. 15.

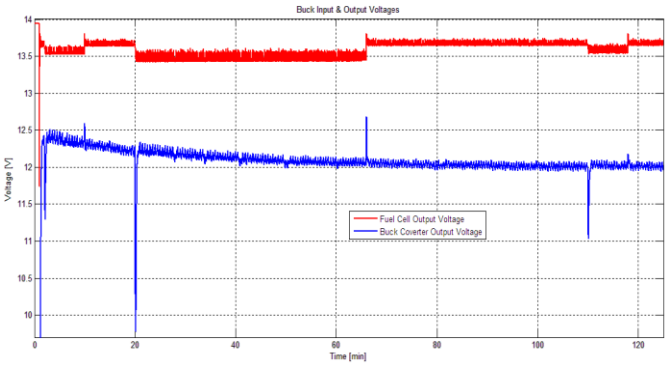


Figure 14. Buck converter input & output voltages

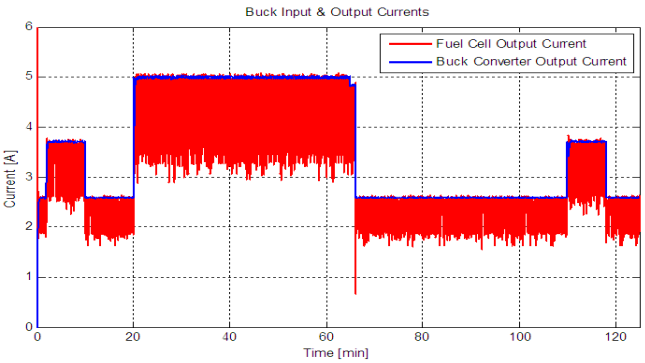


Figure 15. Buck converter input & output currents

## CONCLUSIONS

This paper is concerned with the improvement in overall performance of an electric vehicle propulsion system, which consists of electric energy supply and traction systems. For the traction system, detailed description and mathematical modeling of the BLDC motor and its voltage source inverter are presented. A speed controller is designed successfully using FLC for recovering the actual motor speed to the reference. An optimized PI controller with pulse width modulator is employed for the current control. For the supply system, the operational characteristics and the mathematical modeling of the PEMFC are detailed. A DC-DC buck converter for the fuel cell is built and the selection criterion of its elements is explained. For controlling the buck converter, an optimized PID controller is designed. The parameters of both PI and PID controllers are tuned using gradient-descend multi-parameter-optimization technique. Simulation results verified the capability of the designed PID controller to maintain the output voltage constant under sudden changes in the loads. Several advantages are gained on solving parameter optimization problems using computers; neither reliance on intuition nor experience in control is required, in addition to producing a satisfactory system response with optimal use of effort and time.

## REFERENCES

[1] http://evworld.com/news.cfm?newsid=30499

[2] http://evobsession.com/epri-nrdc-report-mass-adoption-electric-transportation-lead-substantial-reductions-greenhouse-gas-emissions/

[3] L. J. Fu, H. Liu, Y. P. Wu, E. Rahm, R. Holze, and H. Q. Wu, "Surface modifications on electrode materials for lithium ion batteries," Solid State Sci., 2006.

[4] R. Kandiban, and R. Arulmozhiyal, "Design of adaptive fuzzy PID controller for speed control of BLDC motor," vol. 2, Issue-1, March 2012.

[5] A. Emadi, M. Ehsani, and Miller, J. M, "Vehicular electric power systems: land, sea, air, and space vehicles," CRC Press, 2003.

[6] J. Miller, "Propulsion Systems for Hybrid Vehicles," IET, Renewable Energy, 2nd Edition, 2010.

[7] C. P. Singh, SS. Kulkarni, S.C. Rana, and K. Deo, "State-Space based simulink modeling of BLDC motor and its speed control using fuzzy PID controller," International Journal of Advances in Engineering Science and Technology, Vol. 2, Number 3, pp. 359-369,2013.

[8] P. C. K. Luk and C. K. Lee, "Efficient modeling for a brushless DC motor drive," In Industrial Electronics, Control and Instrumentation, 1994. IECON'94., 20th International Conference on. vol. 1. IEEE, 1994.

[9] P. C. Sen, "Principles of electric machines and power electronics," John Wiley & Sons, 1997.

[10] http://media.oem.se/Archive/FilesArchive/29384.pdf

[11] A. Youssef, "Optimized PID tracking controller for piezoelectric hysteretic actuator model," World Journal of Modelling and Simulation, 2013, pp.223-234.

[12] L. Karunarathne, "An Intelligent Power Management System for Unmanned Aerial Vehicle Propulsion Applications," Ph.D. Thesis, Cranfield University, 2012.

[13] S. Mantravadi, "Modeling, Simulation and Implementation of Li-ion Battery Powered Electric and Plug-in Hybrid Vehicles," Master's Thesis, University of Akron, 2011.

[14] J. Meyer, F. Plessis, et al. Aerial Vehicles, " Design considerations for long endurance unmanned aerial vehicles," Intech, 2009.

[15] Committee on Materials, Structures, and Aeronautics Uninhabited Air Vehicles, Uninhabited air vehicles enabling science for military systems, 2000.

[16] N. Safari, "Design of a DC/DC Buck Converter for Ultra-Low Power Applications in 65nm CMOS Process," Master's Thesis, Linköping University, Sweden, 2012.

[17] EG&G Services, "Incorporation Fuel Cell Handbook, Science Applications International Corporation," 2004.

[18] R. Smith, "Design of a control strategy for a fuel cell-battery hybrid power supply," Master's Thesis, Texas A & M University, USA, 2009.